Periodic mesoporous organosilica containing ionic bis-aryl-imidazolium entities: Heterogeneous precursors for silica-hybrid-supported NHC complexes†

Thy Phuong Nguyen,[a] Peter Hesemann,*[a] Philippe Gaveau[b] and Joël J. E. Moreau[a]

Received 9th January 2009, Accepted 31st March 2009
First published as an Advance Article on the web 8th May 2009
DOI: 10.1039/b900431a

The synthesis of periodic mesoporous organosilica incorporating ionic diarylimidazolium species was achieved by hydrolysis–polycondensation of a bis-silylated diarylimidazolium (Si-IMes-) precursor in the presence of non-ionic triblock copolymer as structure directing agents. Although hydrolysis polycondensation of the pure precursor gave materials with moderate porosity, highly porous solids were obtained by the addition of tetraethoxysilane (TEOS) to the sol solution. The architecture of the materials on a mesoscopic scale strongly depends on the TEOS/Si-IMes ratio in the sol. Materials with highly regular hexagonal symmetry were obtained using high molar excess of TEOS. The obtained PMO type materials incorporating diarylimidazolium substructures are promising heterogeneous precursors for the formation of silica hybrid supported *N*-heterocyclic carbene complexes and therefore have great potential in heterogeneous catalysis.

1. Introduction

The synthesis of functional siliceous materials with defined morphologies on a nano- and mesoscopic scale is still a challenge.[1] In the field of silica hybrid materials,[2] periodic mesoporous organosilicas (PMOs) recently emerged as a new class of versatile functional materials.[3] PMO type materials, typically synthesized by hydrolysis–polycondensation of bridged bis-trialcoxysilylated precursor molecules [$(R'O)_3Si–R–Si(OR')_3$] in the presence of structure-directing agents,[4] display two main features which distinguish them fundamentally from other silica based materials, which are: (i) a defined pore architecture on the mesoscopic level, generating high porosity and narrow pore size distribution; and (ii) organic functional groups incorporated in the pore walls, conferring specific properties to the materials. PMOs containing various types of organic substructures have been reported, including small aliphatic, vinylic or aromatic moieties,[5] but also more complex structures such as isocyanurates, dendrimers, fullerenes or chiral groups.[6] PMO type materials have attracted great interest in the last few years owing to their large potential in catalysis,[7] sorption[8] and optics.[9]

Our current interest concerns the elaboration of heterogeneous silica hybrid supported catalysts. Particular attention has been paid on the elaboration of catalytic materials with defined architectures on a nanoscopic level.[10] In this context, we addressed the question of the immobilisation of catalytic species in PMO type materials. We report here the synthesis of nanostructured PMO-type materials bearing bis-aryl imidazolium substructures, which are versatile precursors for the subsequent formation of silica hybrid supported *N*-heterocyclic carbene (NHC) complexes.

The chemical immobilisation of ionic species on solid silica support, introduced by Hölderich *et al.* in 2001,[11] gives rise to versatile materials with large potential in heterogeneous catalysis,[12] chromatography[13] and separation.[14] Most of the reported silica supported ionic phases were obtained by grafting reactions. Reports on PMOs bearing ionic entities obtained by hydrolysis polycondensation of bridged ionic precursors of the type [$(R'O)_3Si$-$\mathbf{R}^+$–$Si(OR')_3$ $\mathbf{X}^-$] are scarce. Dai *et al.* reported silica hybrid material containing di-alkylimidazolium groups but only amorphous materials were obtained.[15] Garcià described MCM-41 type materials bearing viologen and 1,2-bis-(4-pyridyl)ethylene groups,[16] but large excess of silica precursors (tetraethoxysilane, TEOS) were necessary in order to obtain materials with defined architectures on a mesoscopic scale.

Our special concern is the elaboration of silica supported ionic phases with defined architectures. For example, we studied nanostructured silica bearing imidazolium or ammonium entities anchored on the surface of the materials, which were obtained by template directed hydrolysis–polycondensation of trialkoxysilylated precursors.[17] These original materials show interesting morphological features, such as homogeneously distributed ionic

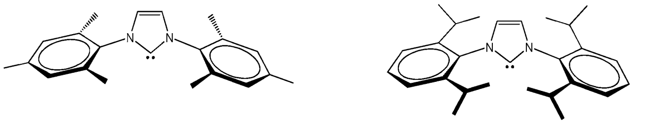

Scheme 1 Chemical structures of the IMes (left) and IPr (right) carbenes.

---

[a]*Institut Charles Gerhardt de Montpellier, UMR CNRS 5253, Equipe Architectures Moléculaires et Matériaux Nanostructurés, 8, rue de l'Ecole Normale, 34296 Montpellier Cedex 05, France. E-mail: peter.hesemann@enscm.fr; Fax: +33 4.67.14.43.53; Tel: +33 (0)4 67 14 72 17*
[b]*Institut Charles Gerhardt de Montpellier, UMR CNRS 5253, Plateau technique, nacelle RMN solide, Place Eugène Bataillon, 34095 Montpellier, France*

† Electronic supplementary information (ESI) available: NMR spectra; adsorption–desorption iostherms. See DOI: 10.1039/b900431a

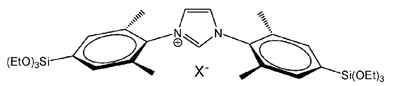

Scheme 2 Chemical structure of the Si-IMes-precursor.

species at the whole silica surface, high porosity and narrow pore-size distribution. Here, we report silica based PMO type materials bearing *N*,*N*′-diarylimidazolium substructures. As compounds of the IMes and IPr family (Scheme 1) are versatile precursors for the formation of metallic NHC complexes PMOs incorporating this type of substructures have great potential in catalysis.[18] In this way, functional materials bearing IMes or IPr substructures may allow the development of heterogeneous NHC catalysts.

We have already reported silica hybrid materials bearing palladium NHC complexes, obtained from silylated bis-alkylimidazolium precursors.[19] Although non-porous and completely amorphous solids, these materials appeared as interesting heterogeneous catalysts for Mizoroki–Heck reactions. However, in view of catalytic versatility and green process engineering, the immobilization of more-active and selective catalytic species within a well-defined solid support becomes an important issue. For this reason, the elaboration of periodic mesoporous organosilicas bearing di-arylimidazolium species is highly desirable, as enhanced catalytic properties related to the IMes or IPr species can be expected. The immobilization of this type of substructure may allow one to perform catalytic processes under milder reaction conditions (time and temperature), thus limiting leaching and enhancing long-lasting stability and recyclability properties of the heterogeneous catalysts. Furthermore, the high degree of molecular rigidity of the IMes or IPr substructures favors the formation of porous solids with well-defined architectures. Contrary to the materials obtained by hydrolysis polycondensation from silylated di-alkyl-imidazolium species, we can expect materials with enhanced catalytic properties due to well-defined architecture of the material on a mesoscopic scale and, therefore, better accessibility of the catalytic sites located at the surface. For this reason, we focused on the synthesis of the silylated Si-IMes precursor (Scheme 2) and, secondly, the formation of porous PMO materials with regular architecture thereof.

2. Experimental

General details

All synthetic procedures were performed under argon using Schlenk-tube techniques. All reagents purchased from commercial sources were used without purification. Glyoxal (40 wt% in water) and chloromethyl pivalate were purchased from Alfa-Aesar, triethoxysilane, bis(acetonitrile) (1,5-cyclooctadiene) rhodium(I) tetrafluoroborate and Pluronic® P-123 were purchased from Aldrich. CTAB and sodium hexadecyl sulfate were purchased from ABCR. 4-Iodo-2,6-dimethylaniline is commercially available, but can easily be prepared by iodination of 2,6-dimethylaniline using iodine monochloride.[20] In experiments requiring dry solvents, THF, toluene and diethylether were distilled from sodium/benzophenone, DMF was distilled from CaH_2, CH_2Cl_2 was distilled from P_2O_5. ^{1}H and ^{13}C spectra in solution were recorded on Bruker AC 250 or Bruker Avance 400 spectrometers at room temperature. Deuterated chloroform was used as solvent for liquid NMR experiments and chemical shifts are reported as δ values in parts per million relative to tetramethylsilane. IR data were obtained on a Perkin–Elmer 1000 FT-IR spectrometer. MS-ESI were measured on a water Q-TOF mass spectrometer.

Syntheses

Synthesis of 4-iodo-2,6-dimethylaniline (2). To a solution of 30.0 g (248 mmol) of 2,6-dimethylaniline (**1**) dissolved in a mixture of 450 mL methanol–dichloromethane (450 mL, 1 : 1) is added a solution of 40.2 g (248 mmol) of iodochloride dissolved in 50 mL in a mixture methanol–dichloromethane (1 : 1). The reaction mixture was stirred during 24 h at room temperature. After this time, the solvents were evaporated. The crude solid product was treated with 200 mL of an aqueous sodium hydroxide solution (20 wt%) and finally extracted with diethylether (3 × 150 mL). After drying over sodium sulfate, the product solution was filtered and the organic solvent was evaporated. The pure title compound **2** was obtained after distillation *in vacuo* (0.01 mbar, T_{eb} 99–103 °C) as a brownish oil, which cristallized upon standing at room temperature. Yield: 30.6 g (50%). ^{1}H NMR ($CDCl_3$) δ 2.05 (s, 6H), 3.43 (s, 2H), 7.19 (s, 2H); ^{13}C NMR ($CDCl_3$): δ 17.3, 79.2, 124.2, 136.4, 142.5.

Synthesis of bis(4-iodo-2,6-dimethylphenyl)diazabutadiene (3). A 500 ml round-bottom flask was charged with 15.86 g (64.2 mmol) of 4-iodo-2,6-dimethylaniline, 4.5 mL (31 mmol, 40% in water) of glyoxal and 150 ml of methanol. A few drops of formic acid were added as catalyst. The color of the reaction mixture turned from colorless to yellow immediately, and a yellow precipitate appeared after a few hours. The reaction mixture was stirred for two days and the yellow solid was collected by filtration and washed with cold methanol to afford the analytically pure **3**. Yield: 11.29 g (21.9 mmol, 71%). ^{1}H NMR ($CDCl_3$) δ 2.05 (s, 12H), 7.37 (s, 4H), 7.99 (s, 2H); ^{13}C NMR ($CDCl_3$): δ; 17.90, 89.09, 128.86, 136.95, 149.46, 163.50; FT-IR(KBr) ν_{max}/cm^{-1} 2966, 2919, 2856, 1616, 1568, 1466, 1181, 855.

Synthesis of 1,3-bis(4-iodo-2,6-dimethylphenyl)-1*H*-imidazol-3-ium trifluoromethanesulfonate (4). To a solution of the bis-imine **3** (2.00 g/3.86 mmol) in 30 mL of dichloromethane were added 0.9 mL (0.94 g/6.25 mmol) chloromethyl pivalate and finally 1.28 g (5 mmol) silver trifluoromethanesulfonate. The resulting reaction mixture was heated to reflux over 18 h. After cooling to room temperature, the formed precipitate (silver chloride) was eliminated by filtration. The homogeneous solution was concentrated giving the crude product as a brown residue, which was dissolved in 5 mL of methanol. The pure title compound was obtained as an off-white solid by precipitation in diethyl ether, filtration and drying under vacuum. Yield: 2.05 g (78%). ^{1}H NMR ($CDCl_3$) δ 2.04 (s, 12H), 7.51 (d, 2H, J = 1.5 Hz), 7.55 (s, 4H), 9.49 (t, 1H, J = 1.6 Hz); ^{13}C NMR (DMSO): δ 16.52, 97.75, 120.56 (q, CF_3, J = 322 Hz) 124.67, 133.23, 137.04, 137.33.12, 138.24; FT-IR(KBr) ν_{max}/cm^{-1} 3172, 3112, 3046, 2925, 1573, 1548, 1454, 1285, 1213, 1154, 1028; HRMS [ESI+] calcd for $C_{19}H_{19}N_2I_2$ (cation) 528.9638, found 528.9651.

Synthesis of 1,3-bis(4-triethoxysilyl-2,6-dimethylphenyl)-1*H*-imidazol-3-ium trifluoromethane-sulfonate (5). 434 mg (0.64 mmol) of the bis-iodinated compound **4** and 12.1 mg of Rh(cod)$(CH_3CN)_2$ BF_4 (0.032 mmol) were dissolved in 5 mL of DMF. To this homogeneous solution were added 1 mL (0.727 g/7.2 mmol) of triethylamine and 1 mL (0.89 g/5.4 mmol) of triethoxysilane. The resulting solution was heated with stirring to 80 °C over 4 h. After cooling, the solvents were pumped off and the brown residue was dissolved in 40 mL of dichloromethane. The formed ammonium salts were eliminated by extraction with cold water (2 × 30 mL). The organic phase was dried over sodium sulfate and filtered. After concentration, the imidazolium salt was precipitated in a diethyl ether–pentane mixture (50/50) to afford the pure title compound after filtration and drying under vacuum. Yield: 350 mg (0.47 mmol, 73%). ^{1}H NMR ($CDCl_3$) δ 1.30 (t, 18H, J = 7.1 Hz), 2.56 (bs, 3H), 2.25 (s, 12H), 3.92 (q, 12H, J = 7.1 Hz), 7.58 (s, 4H), 7.65 (d, 2H, J = 1.6 Hz), 9.86 (t, 1H, J = 1.6 Hz); ^{13}C NMR ($CDCl_3$): δ 17.49, 18.22, 58.98, 124.94, 133.54, 134.48, 135.67, 135.75, 137.42; FT-IR(KBr) ν_{max}/cm^{-1} 3112, 3079, 2977, 2927, 2894, 1541, 1284, 1163, 1103, 1077; HRMS [HR-ESI+] calcd for $C_{31}H_{49}N_2O_6Si_2$ (cation) 601.3129, found 601.3144.

Materials' synthesis. All materials were synthesized following standard reaction conditions. Table 1 and 2 give detailed information about the used quantities for the syntheses for the pure gels **A**–**D** and co-gels **A1/2**–**A1/9** The sol solutions were vigorously stirred at 45 °C over 15 h and then aged without stirring over 48 h. After hydrolysis/polycondensation, the formed solids were collected by filtration and intensively washed with copious amounts of water. Surfactants were eliminated by washing the solids in a Soxhlet apparatus over 24 h using a mixture of 200 mL of ethanol and 3 mL conc. hydrochloric acid. The obtained solids were finally dried in a vacuum oven at 70 °C over 24 h.

Characterization of the PMO-materials. Solid state ^{13}C and ^{29}Si CP MAS NMR experiments were recorded on a Varian VNMRS 400MHz solid spectrometer using a two channel probe with 7.5 mm ZrO_2 rotors. Nitrogen sorption isotherms at 77 K were obtained with a Micromeritics Tristar apparatus. Prior to measurement, the samples were degassed for 18 h at 100 °C. The surface area (S_{BET}) were determined from BET treatment in the range 0.04–0.3 p/p_0[21] and assuming a surface coverage of nitrogen molecule estimated to 13.5 Å^2. Pore size distributions were calculated from the adsorption branch of the isotherms using the BJH method. TEM images were obtained using JEOL 1200 EX II (120kV). XRD experiments were carried out with a Xpert-Pro (PanAnalytical) diffractometer equipped with a fast X'celerator detector using Cu Kα radiation.

3. Results and discussion

Precursor synthesis

Prior to the materials synthesis, we initially focused on the synthesis of the ionic Si-IMes precursor, which was achieved in a four-step sequence starting from 2,6-dimethylaniline **1**. The reaction sequence is represented in Scheme 3. At first, iodination of 2,6-dimethylaniline **1** with iodine monochloride gave the corresponding 4-iodo-2,6-dimethylaniline **2**.[20] In a second step, this compound was reacted with glyoxal to yield the bis-imine **3**.[22] Ring closing was then achieved using the standard conditions first reported by Glorius *et al.*[23] and recently used by Douce *et al.* for the synthesis of related liquid crystalline *N*,*N'*-diaryl-imidazolium species.[24] This reaction occurred smoothly with chloromethyl pivalate in the presence of silver triflate to give the imidazolium derivative **4**.

Silylation was finally realized *via* rhodium catalyzed cross-coupling of aryliodides with triethoxysilane (Scheme 4).[25] This useful reaction appeared as a versatile method in order to promote C_{aryl}–Si coupling reactions under mild reaction conditions in short reaction times. Silylation applied on the di-iodo imidazolium precursor **4** afforded the ionic Si-IMes precursor **5** in high selectivity and good yield. It is noteworthy that other silylation reactions gave unsatisfactory results. In previous studies, we reported silylation of aromatic rings by Heck-reaction or by coupling of metalated intermediates with silyl electrophiles.[26] These procedures applied on this ionic di-iodinated

Table 1 Composition of the sol solutions for preparing the pure gels **A**–**D**

Material	Precursor quantity	Surfactant (quantity)	Solvent
A	400 mg	P123 (208 mg)	2 N hydrochloric acid (6.4 mL)
B	400 mg	C16-sulfate (87 mg)	2 N hydrochloric acid (6.4 mL)
C	500 mg	—	EtOH(2 mL) + TBAF (13μL, 1 N soln. in THF)
D	150 mg	CTAB (83 mg)	3.9 N ammoniac solution (4.1 mL)

Table 2 Composition of the sol solutions for preparing the pure gels **A1/2**–**A1/9**

	Precursor quantity		TEOS			
Material	Mass/mg	mmol	Mass/mg	mmol	Surfactant (quantity)	Reaction medium (volume)
A1/2	175	0.23	97	0.47	P123 (91 mg)	2 N hydro-chloric acid (2.8 mL)
A1/3	250	0.33	208	1	P123 (224 mg)	2 N hydro-chloric acid (6.9 mL)
A1/4	250	0.33	277	1.33	P123 (250 mg)	2 N hydro-chloric acid (7.7 mL)
A1/6	250	0.33	415	2	P123 (304 mg)	2 N hydro-chloric acid (9.4 mL)
A1/9	137	0.18	342	1.64	P123 (213 mg)	2 N hydro-chloric acid (6.6 mL)

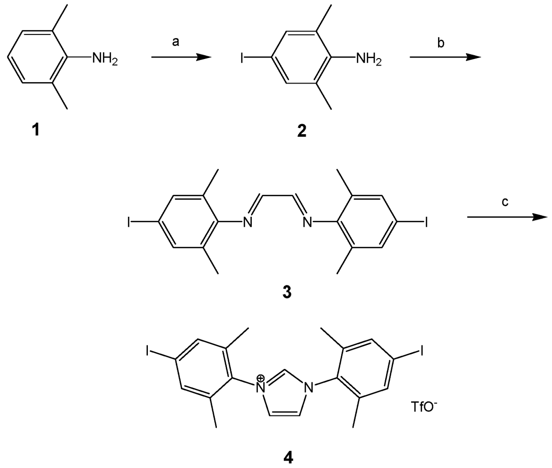

Scheme 3 Reactions and conditions: (a) MeOH–CH_2Cl_2, ICl; (b) glyoxal, MeOH, cat. HCOOH; (c) THF, chloromethyl pivalate, silver triflate.

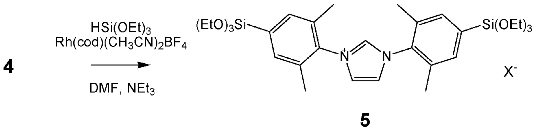

Scheme 4 Synthesis of the Si-IMes precursor **5** by rhodium-catalyzed Si–C coupling.

precursor molecule **4** failed, probably due to decomposition of the central imidazolium entity under strongly basic reaction conditions. Thus, Rh catalyzed silylation appeared as most useful option and afforded the best results in terms of yield and purity of the obtained reaction products.

The silylation reaction occurred smoothly and gave the Si-IMes **5** in satisfactory yield. The treatment of the crude reaction mixture with a biphasic water–dichloromethane (DCM) mixture allowed to separate the water-soluble triethylammonium iodide, formed during the silylation reaction, and DCM-soluble precursor **5**. The Si-IMes precursor **5** was finally precipitated in an ether/pentane mixture and isolated after filtration and drying.

Synthesis of pure hybrid materials

The Si-IMes precursor **5** was subsequently used for the synthesis of silica hybrid materials. In the first series of experiments, hybrid materials were synthesized from the pure Si-IMes precursor under different hydrolysis–polycondensation conditions in order to get more detailed information about their chemical stability. These reactions were carried out either in template-directed hydrolysis polycondensation in the presence of cationic (CTAB), anionic (C16-sulfonate) and non ionic (P123) surfactants or under nucleophilic catalysis of fluoride ions, without structure directing agents (Table 3).

Table 3 Synthesis conditions and morphological features of the hybrid materials **A**–**D**

Material	Surfactant	Hydrolysis polycondensation conditions	Specific surface area/m^2 g^{-1}
A	P123	Acidic/HCl	104
B	C16-sulfonate	Acidic/HCl	57
C	—	Neutral/F^-	7
D	CTAB	Basic/NH_4OH	Decomp. of the Si-IMes substructure

In order to study the chemical stability of the precursor under different hydrolysis–polycondensation conditions, the obtained materials **A**–**D** were characterized by ^{29}Si solid state NMR spectroscopy. The spectra of materials **A** and **D**, obtained by CP-MAS techniques, are shown as examples in Fig. 1. The spectrum of material **A** revealed the signals of the T-series corresponding to hydrolyzed R-SiO_3 substructures with different condensation degree. The highest intensity was observed for the T^2-signal corresponding to R–$Si(OH)_1(OSi)_2$ substructures. Similar results were obtained with materials **B** and **C** (see the ESI†). All three spectra also displayed very weak Q-peaks, corresponding to the presence of a small amount (approx. 5%) of SiO_4 substructures in the gels, formed by Si–C bond cleavage during hydrolysis–polycondensation.

Contrary to these results, the spectra of material **D**, obtained by hydrolysis–polycondensation of the precursor in basic medium, shows much more intense Q-resonances (Fig. 1, top). This first result indicate considerable Si–C bond cleavage caused by nucleophilic attack of hydroxide ions on the silicon attached to the organic substructures followed by Si–C scission. Silicon-carbon bond cleavage in lower extent has already been observed during hydrolysis–polycondensation of phenylene and biphenylene precursors in basic media.[27] However, the high degree of bond scission observed using the Si-IMes precursor **5** highlights a weakening effect of the ionic imidazolium entities on the C–Si bond located in *para*-position.

The chemical integrity of the imidazolium substructures in materials **A**–**C** was proved by ^{13}C CP-MAS spectroscopy. Fig. 2 represents the superposed ^{13}C liquid NMR spectrum of the Si-IMes precursor **5** (bottom) and ^{13}C CP-MAS spectrum of material **A** (top). The spectrum of the ionic precursor shows the signals of the methyl groups on the aromatic rings at 17.5 ppm and the signals of the two aryl and the central imidazolium rings in the range 125–140 ppm. Intense signals at 18 and 59 ppm are due to $(EtO)_3Si$ groups. Complete disappearance of these latter signals in the solid state spectrum of material **A** indicates total

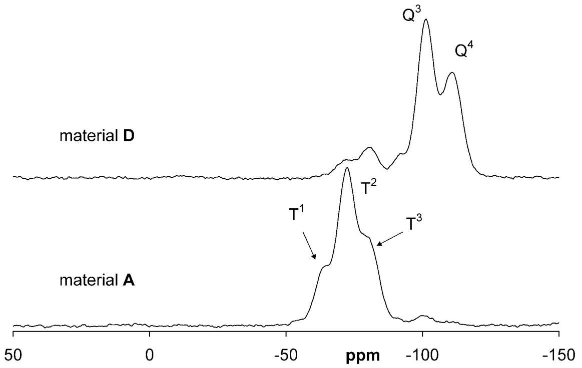

Fig. 1 ^{29}Si CP MAS solid state NMR spectra of materials A (bottom) and D (top).

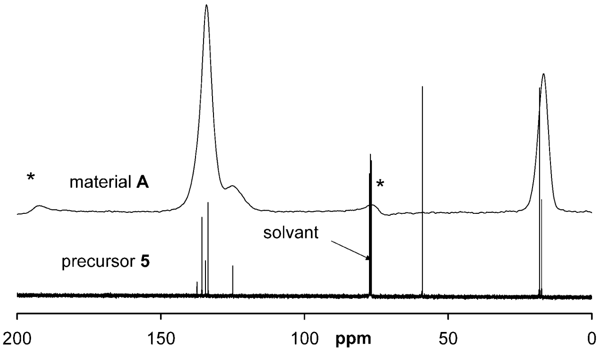

Fig. 2 ^{13}C liquid NMR spectrum of the Si-IMes precursor 5 (bottom) and ^{13}C CP-MAS solid state NMR spectrum of material A (top); spinning side bands are marked with asterisks.

hydrolysis of these groups. The resonances at 17 and 125–134 ppm observed in the solid state NMR spectrum of materials **A** are in nice agreement with the chemical shifts observed in the liquid NMR spectrum of the precursor and indicate the sufficient chemical stability of the organic substructure of the Si-IMes precursor towards the hydrolysis–polycondensation conditions. Finally, the absence of further signals in the spectrum of material **A** indicates the complete elimination of structure directing agents (P123) used for the synthesis of the material.

Contrary to these results, the ^{13}C CP-MAS spectrum of material **D** (see the ESI†) shows additional signals at 30 and 52 ppm indicating chemical degradation of the IMes substructure. Thus, the precursor **5** undergoes not only Si–C bond cleavage in basic reaction media, but secondly degradation of the ionic substructure, probably induced by deprotonation of the C2 carbon on the imidazolium ring. These results reflect the limited stability of imidazolium species in basic reaction media, already observed for bis-alkyl-imidazolium salts.[28]

These results suggest that the IMes substructure is preserved in the materials **A**–**C**, synthesized in acidic and neutral reaction media, whereas chemical degradation and Si–C bond cleavage occur when hydrolysis–polycondensation is carried out in basic reaction media. Following these results, hydrolysis–polycondensation of the precursor **5** in basic media was not further considered, and further analytic data were collected only for the materials **A**–**C**. XRD experiments with these materials showed no diffraction rays, indicating formation of amorphous solids. Nitrogen sorption experiments showed that the hybrid materials **A**–**C** are solids with specific surface areas of 7 m^2 g^{-1} for material **C** and up to 104 m^2 g^{-1} observed for material **A**. In conclusion, the hybrid materials synthesized by hydrolysis–polycondensation of the ionic Si-IMes precursor **5** in acidic or neutral media are completely amorphous solids with low to moderate porosity. The use of non-ionic surfactants is the best choice in order to generate porosity in PMO type materials bearing ionic IMes substructures.

Synthesis of PMO type materials

In a second set of experiments, we synthesized periodic mesoporous organosilica by co-condensation of the ionic Si-IMes precursor **5** with various amounts of tetraethoxysilane (TEOS).

Following the previously obtained results for the hydrolysis–polycondensation of the pure precursor **5** in different reaction media, we carried out these reactions in acidic solution using non-ionic triblock copolymer P123 as structure directing agent as described for the synthesis of material **A**. The different molar ratios of Si-IMes precursor **5** and TEOS in the sol solutions are as 1 : 2, 1 : 3, 1 : 4, 1 : 6 and 1 : 9, giving rise to the formation of the materials **A1/2**, **A1/3**, **A1/4**, **A1/6** and **A1/9**.

The obtained materials were analyzed by solid state NMR spectroscopy, elemental analysis, XRD and nitrogen sorption experiments. ^{29}Si CP-MAS NMR spectra of the materials (Fig. 3) showed both the signals of the T and Q-series in the gels due to the presence of R–SiO$_3$ and SiO$_4$ substructures in the gels. In all gels, the major environment of the silicon correspond to T^3 and Q^3 species. The spectra show increasing intensities of the signals of the Q^n series with increasing amount of TEOS used for the synthesis of the materials. Even if the CP technique is not quantitative, it can be sufficiently precise to compare the materials in order to get quantitative information about the ratio between RSiO$_3$- and SiO$_4$-substructures in the cogels (T^n/Q^n-ratio). As shown in Table 4, integration over the T and Q resonances in the spectra of materials **A1/2**, **A1/3** and **A1/9** are in good agreement with the theoretical values and suggest correct incorporation of the imidazolium substructures within the cogels.

Elemental analyses of the materials (Table 5) confirm the incorporation of the ‘organo-ionic’ precursor in the PMO type materials. The found carbon and nitrogen values generally fit well the calculated values and reflect the different amounts of incorporated imidazolium substructures in the solids. These results exclude the presence of residual triethoxysilyl groups in the materials in agreement of the results obtained by ^{13}C solid state NMR spectroscopy. The found hydrogen contents of the

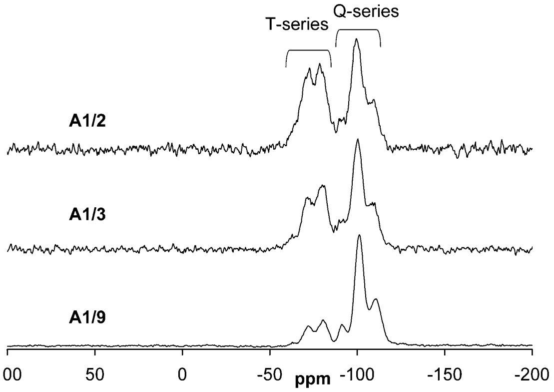

Fig. 3 ^{29}Si CP-MAS solid state NMR spectra of the materials **A1/9** (bottom), **A1/3** (center) and **A1/2** (top).

Table 4 Calculated and found T^n/Q^n values in the cogels

Material	T^n/Q^n ratio (calc.)	T^n/Q^n ratio (found)
A1/9	18/82	22/78
A1/3	40/60	42/58
A1/2	50/50	51/49

Table 5 Elemental analyses of the materials

	Calculated values			Found values		
Material	C	H	N	C	H	N
A	45.06	3.78	5.53	46.21	5.15	5.58
A1/2	36.42	3.06	4.47	35.74	4.86	4.06
A1/3	33.23	2.79	4.08	32.71	4.46	3.65
A1/4	30.56	3.75	2.56	33.25	4.39	3.73
A1/6	26.32	2.21	3.23	26.22	3.86	2.79
A1/9	21.79	1.83	2.68	24.10	3.84	2.19

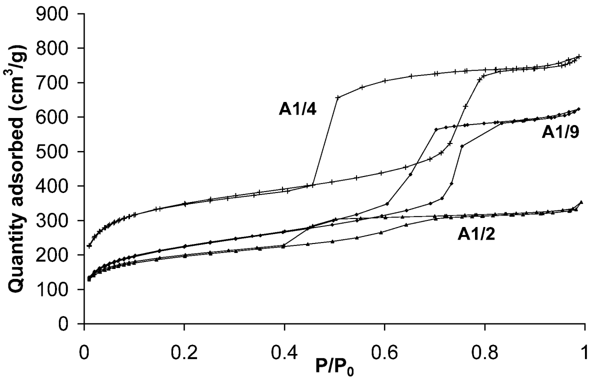

Fig. 4 Nitrogen sorption isotherms of the materials **A1/2** (bottom, ▲), **A1/9** (center, ◆) and **A1/4** (top, +). Isotherms of materials **A1/6** and **A1/3** are omitted for clarity and given in the ESI.†

materials are slightly higher than the calculated values due to the presence of non condensed silanol groups as indicated by ^{29}Si solid state NMR spectroscopy.

Nitrogen adsorption desorption isotherms of the materials **A1/9**, **A1/4** and **A1/2** are shown in Fig. 4, and the isotherms of materials **A1/6** and **A1/3** are given in the ESI.† Principal results are summarized in Table 6. The isotherms indicate that all cogels obtained by hydrolysis–polycondensation of precursor **5** with various amounts of TEOS are highly porous materials with specific surface areas in the range from 720 to 1170 m^2 g^{-1}. The presence of hysteresis loops indicate mesoporosity in all materials. A trend was observed concerning the average pore diameters of the materials, which were obtained from the adsorption branches of the isotherms using the BJH method. The shape of the isotherms reveals a typical SBA-15 type morphology in the case of **A1/9** and **A1/6** in terms of porous volume (0.96/0.92 cm^3 g^{-1}) and average pore size diameter (60/72 Å). The observed results for material **A1/9** are in nice agreement with pure SBA-15 silica obtained by hydrolysis–polycondensation of TEOS under similar conditions using P123 as template.[29] The results obtained for the materials **A1/4**, **A1/3** and **A1/2** suggest that the pore diameters decrease with lower amount of TEOS in the sol. In the case of materials **A1/3** and **A1/4**, the observed average pore sizes are slightly lower (55 Å/54 Å) and reached a final value of 40 Å in the case of material **A1/2**.

Table 6 Morphological features of the cogels obtained from nitrogen sorption experiments

Material	Specific surface area/m^2 g^{-1}	Pore volume/cm^3 g^{-1}	Average pore diameter/Å^a
A1/2	720	0.55	40
A1/3	920	0.90	55
A1/4	1170	1.20	54
A1/6	779	0.92	72
A1/9	815	0.96	60

^{a} Average pore sizes were calculated from the adsorption branch of the nitrogen sorption isotherm.

Concerning porosity of the materials, a maximum specific surface value with 1170 m^2 g^{-1} was observed for the material **A1/4**. The other materials showed lower surface areas in the range from 700–900 m^2 g^{-1}. According to these results, material **A1/4** also shows the highest pore volume in this series. In conclusion, the ratio between precursor **5** and TEOS in the sol has deep influence on the morphology of the formed solid in terms of specific surface area and pore diameter.

XRD experiments with the cogels were performed in order to get deeper insight in the texture of the materials on a mesoscopic scale. The diffractograms of the materials **A1/9**, **A1/6**, **A1/4**, **A1/3** and **A1/2** are shown in Fig. 5. Intense reflections at small angles show relatively similar *d*-spacings in this series of materials in the range of 105 to 125 Å, corresponding to interpore distances of 121–144 Å. The thickness of the pore walls in the materials was estimated as being the difference between the interpore distances obtained from from the XRD and the pore diameters obtained from the adsorption branch of the nitrogen sorption isotherms. These results suggest that the wall thickness of the materials bearing ionic imidazolium entities slightly increases with increasing amount of the Si-IMes precursor in the sol solution (Table 7).

Concerning the architecture of the materials on a mesoscopic scale, the diffractogram of material **A1/9** showed the (100), (110) and (200) reflections characteristic for materials with hexagonal symmetry. Material **A1/6** gave a similar diffractogram with

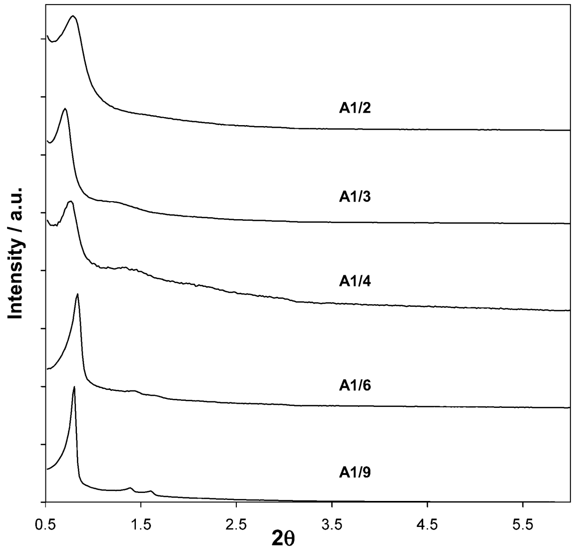

Fig. 5 XRD diffractograms of the materials **A1/9**, **A1/6**, **A1/4**, **A1/3** and **A1/2** (bottom to top).

Table 7 Summarized morphological features of the materials obtained from XRD and nitrogen sorption experiments

Material	Interpore distance	Average pore diameter/Å[a]	Estimated wall thickness/Å
A1/2	129	40	89
A1/3	144	55	89
A1/4	131	54	77
A1/6	121	72	49
A1/9	127	60	67

[a] Average pore sizes were calculated from the adsorption branch of the nitrogen sorption isotherm.

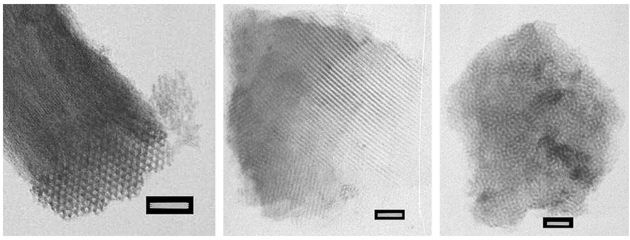

Fig. 6 TEM micrographs of materials **A1/9** (left/middle) and **A1/3** (right); bar: 50 nm.

nearly identical reflection angles. However, the reflections in the case of materials **A1/6** are less well-defined, indicating lower structural regularity compared to material **A1/9**. In the diffractograms of materials **A1/4**, **A1/3** and **A1/2**, the (110) and (200) reflections completely disappear, indicating less defined architectures and wormlike structures in the materials.

These results are confirmed by transmission electron microscopy (TEM). TEM images of materials **A1/9** and **A1/3** are given as examples in Fig. 6. The micrograph of material **A1/9** shows a regular hexagonal array of 2d-aligned pores as expected for SBA-15 related materials. Contrary to this, the TEM micrographs of materials **A1/3** clearly displays high porous character of the material, but at the same time irregular arrangement of the pore structure. However, the pore size distribution is relatively narrow as indicated from the nitrogen sorption experiments.

These results show that ionic Si-IMes substructures can be incorporated into mesoporous SBA-15 related materials using a non-ionic triblock copolymer surfactant as a structure-directing agent. The materials obtained by hydrolysis polycondensation with various amounts of TEOS all exhibit high porosity, even those with a very high content of the ionic substructure. However, structural regularity decreases with increasing amount of incorporated imidazolium substructures.

4. Conclusion

We report the synthesis of a bis-triethoxysilylated imidazolium triflate precursor and the synthesis of PMO type materials thereof. Hydrolysis–polycondensation in acidic and neutral media led to the formation of silica hybrid materials incorporating the ionic substructure whereas sol–gel procedures in basic media led to chemical decomposition as well as to carbon–silicon cleavage of the precursor. Cogels were obtained from the ionic precursor and various amounts of tetraethoxysilane (TEOS). The obtained materials displayed high porosity even with high content of the ionic substructure, due to the high degree of molecular rigidity of the ionic precursor. However, in the case of the materials containing high degrees of organic parts and, consequently, low silica content, the structural regularity decreased.

The reported materials are versatile precursors for the generation of silica hybrid supported *N*-heterocyclic carbene complexes and have large potential for the elaboration of recyclable heterogeneous catalysts. We are currently investigating these materials for applications in Pd-catalyzed C–C cross coupling reactions. These results will be reported in due course.

Acknowledgements

The authors gratefully acknowledge Eva Rettenmeier for technical assistance. P. Hesemann thanks the ‘Groupement de Recherche PARIS’ and the ‘Réseau de Recherche 3, Chimie pour le Développement Durable ’ of the CNRS for financial support.

References

1 G. J. A. A. Soler-Illia, C. Sanchez, B. Lebeau and J. Patarin, *Chem. Rev.*, 2002, **102**, 4093–4138; F. Hoffmann, M. Cornelius, J. Morell and M. Froba, *Angew. Chem., Int. Ed.*, 2006, **45**, 3216–3251.

2 K. J. Shea, D. A. Loy and O. J. Webster, *J. Am. Chem. Soc.*, 1992, **114**, 6700–6710; R. J. P. Corriu, J. J. E. Moreau, P. Thépot and M. Wong Chi Man, *Chem. Mater.*, 1992, **4**, 1217–1224.

3 S. Inagaki, S. Guan, Y. Fukushima, T. Ohsuna and O. J. Terasaki, *J. Am. Chem. Soc.*, 1999, **121**, 9611–9614; B. J. Melde, B. T. Holland, C. F. Blanford and A. Stein, *Chem. Mater.*, 1999, **11**, 3302–3308; T. Asefa, M. J. MacLachlan, N. Coombs and G. A. Ozin, *Nature*, 1999, **402**, 867–871.

4 S. Fujita and S. Inagaki, *Chem. Mater.*, 2008, **20**, 891–908.

5 O. Muth, C. Schellbach and M. Froba, *Chem. Commun.*, 2001, 2032–2033; K. Landskron, B. D. Hatton, D. D. Perovic and G. A. Ozin, *Science*, 2003, **302**, 266–269; C. Vercaemst, M. Ide, B. Allaert, N. Ledoux, F. Verpoort and P. Van der Voort, *Chem. Commun.*, 2007, 2261–2263; S. Bracco, A. Comotti, P. Valsesia, B. F. Chmelka and P. Sozzani, *Chem. Commun.*, 2008, 4798–4800.

6 C. Baleizao, B. Gigante, D. Das, M. Alvaro, H. Garcia and A. Corma, *Chem. Commun.*, 2003, 1860–1861; K. Landskron and G. A. Ozin, *Science*, 2004, **306**, 1529–1532; O. Olkhovyk and M. Jaroniec, *J. Am. Chem. Soc.*, 2005, **127**, 60–61; W. Whitnall, L. Cademartiri and G. A. Ozin, *J. Am. Chem. Soc.*, 2007, **129**, 15644–15649.

7 Q. Yang, J. Liu, J. Yang, M. P. Kapoor, S. Inagaki and C. Li, *J. Catal.*, 2004, **228**, 265–272.

8 V. Rebbin, R. Schmidt and M. Fröba, *Angew. Chem., Int. Ed.*, 2006, **45**, 5210–5214.

9 P. N. Minoofar, R. Hernandez, S. Chia, B. Dunn, J. I. Zink and A.-C. Franville, *J. Am. Chem. Soc.*, 2002, **124**, 14388–14396.

10 R. Ciriminna, P. Hesemann, J. J. E. Moreau, M. Carraro, S. Campestrini and M. Pagliaro, *Chem.–Eur. J.*, 2006, **12**, 5220–5224; V. Polshettiwar, P. Hesemann and J. J. E. Moreau, *Tetrahedron*, 2007, **63**, 6784–6790; X. Elias, R. Pleixats, M. Wong Chi Man and J. J. E. Moreau, *Adv. Synth. Catal.*, 2007, **349**, 1701–1713.

11 M. H. Valkenberg, C. deCastro and W. F. Hölderich, *Green Chem.*, 2002, **4**, 88–93.

12 C. P. Mehnert, *Chem.–Eur. J.*, 2005, **11**, 50–56, and references therein; T. Sasaki, C. Zhong, M. Tada and Y. Iwasawa, *Chem. Commun.*, 2005, 2506–2508; M. Gruttadauria, S. Riela, C. Aprile, P. Lo Meo, F. D’Anna and R. Noto, *Adv. Synth. Catal.*, 2006, **348**, 82–92.

13 S.-J. Liu, F. Zhou, L. Zhao, X. H. Xiao, X. Liu and S.-X. Jiang, *Chem. Lett.*, 2004, **33**, 496–497.

14 Y. H. Ju, O. F. Webb, S. Dai, J. S. Lin and C. E. Barnes, *Ind. Eng. Chem. Res.*, 2000, **39**, 550–553.

15 B. Lee, H.-J. Im, H. Luo, E. W. Hagaman and S. Dai, *Langmuir*, 2005, **21**, 5372–5376.

16 M. Alvaro, B. Ferrer, H. Garcia and F. Rey, *Chem. Commun.*, 2002, 2012–2013; M. Alvaro, B. Ferrer, V. Fornes and H. Garcia, *Chem. Commun.*, 2001, 2546–2547.

17 B. Gadenne, P. Hesemann and J. J. E. Moreau, *Chem. Commun.*, 2004, 1768–1769; B. Gadenne, P. Hesemann, V. Polshettiwar and J. J. E. Moreau, *Eur. J. Inorg. Chem.*, 2006, 3697–3702; V. Polshettiwar, P. Hesemann and J. J. E. Moreau, *Tetrahedron*, 2007, **63**, 6784–6790.

18 *N-Heterocyclic Carbenes in Synthesis*, ed. S. P. Nolan, Wiley-VCH, Weinheim, Germany, 2006.

19 V. Polshettiwar, P. Hesemann and J. J. E. Moreau, *Tetrahedron Lett.*, 2007, **48**, 5363–5366.

20 Z.-L. Lu, A. Mayr and K. K. Cheung, *Inorg. Chim. Acta*, 1999, **284**, 205–214.

21 S. Brunauer, P. H. Emmett and E. J. Teller, *J. Am. Chem. Soc.*, 1938, **60**, 309–319.

22 I. G. Jung, J. Seo, Y. K. Chung, D. M. Shin, S.-H. Chun and S. U. Son, *J. Polym. Sci., Part A: Polym. Chem.*, 2007, **45**, 3042–3052.

23 F. Glorius, G. Latenhoff, R. Goddard and C. Lehmann, *Chem. Commun.*, 2002, 2704–2705.

24 J.-M. Suisse, S. Bellemin-Laponnaz, L. Douce, A. Maisse-François and R. Welter, *Tetrahedron Lett.*, 2005, **46**, 4303–4305; J.-M. Suisse, L. Douce, S. Bellemin-Laponnaz, A. Maisse-François, R. Welter, Y. Miyake and Y. Shimizu, *Eur. J. Org. Chem.*, 2007, 3899–3905.

25 M. Murata, H. Yamasaki, T. Ueta, M. Nagata, M. Ishikura, S. Watanabe and Y. Masuda, *Tetrahedron*, 2007, **63**, 4087–4094.

26 A. Brethon, P. Hesemann, L. Rejaud, J. J. E. Moreau and M. W. C. Man, *J. Organomet. Chem.*, 2001, **627**, 239–248.

27 K. Okamoto, Y. Goto and S. Inagaki, *J. Mater. Chem.*, 2005, **15**, 4136–4140.

28 V. K. Aggarwal, I. Emme and A. Mereu, *Chem. Commun.*, 2002, 1612–1613.

29 D. Zhao, Q. Huo, J. Feng, B. F. Chmelka and G. D. Stucky, *J. Am. Chem. Soc.*, 1998, **120**, 6024–6036.